International Journal of Optics and Applications 2015, 5(2): 33-49
DOI: 10.5923/j.optics.20150502.02

Optical and Structural Characterization of Diffuse Reflectance Standards

Antonio Parretta[1,2,*], Maria Luisa Addonizio[3]

[1]Physics and Earth Science Department, University of Ferrara, Via Saragat 1, 44122 Ferrara (FE), Italy
[2]ENEA Centro Ricerche "E. Clementel", Via Martiri di Monte Sole 4, 40129 Bologna (BO), Italy
[3]ENEA Centro Ricerche Portici, P.le Enrico Fermi, 1, 80055 Portici (NA), Italy

Abstract In this paper, we describe the optical properties of Labsphere diffuse reflectance standards of different nominal reflectance. Specifically, we analyze their properties of hemispherical total reflectance and angular distribution of scattered light intensity, as function of the angle of incidence and wavelength of a laser beam. Our main objective is to find the difference between the optical behavior of a real diffuser of given average reflectance and that of an ideal Lambertian diffuser. The optical characterizations were carried out by using original methods and apparatus, and were followed by SEM-EDS analysis with the aim to relate the optical properties with the morphological and structural characteristics. The optical characterizations demonstrate that the standards with high nominal total reflectance approach better the Lambertian behavior. This result is confirmed by SEM analysis, showing, for these samples, the most rugged surfaces and a porous material.

Keywords Reflectance standard, Optical diffuser, Optical characterization, Integrating sphere, SEM analysis

1. Introduction

Reflectance standards are commonly used in commercial spectrophotometers for calibration purposes and the most widely used ones are those with high reflectivity (close to 99%) in the visible and near-infrared range, showing almost ideal reflection properties, those of a Lambertian diffuser [1]. Reflectance standards are also key components in optical laboratories devoted to the characterization of materials and devices for solar energy research [2-13]. In this work we investigate the optical properties of standards with very different nominal reflectivity, in particular a series produced by Labsphere, which cover the range of values from about 2% to about 99%. Our interest for these light diffusers comes from their intensive use with the innovative equipments developed in the past years at ENEA-Portici and Ferrara University labs, and devoted to the non-destructive optical characterization of photovoltaic materials and devices [4-20]. These devices are realized with textured surfaces, to better absorb solar radiation, and have been studied in terms of total or diffuse reflectance and spatial distribution of the diffused light [21-25]. Since these devices are very little reflective, it is advantageous to perform the calibration measurements with standards of similar reflectivity in order to improve the accuracy of measurements. We used reflectance standards also to analyze the flux distribution on cross-sections of focused solar beams produced by CPV (Concentrating Photovoltaics) systems, following the so called camera-target or light scattering-CCD method [26-28]. Here, the standard diffuser intercepts the light beam while a CCD camera records the image of the irradiated surface. The analysis of the image allows, after appropriate processing [28], to recover the flux density distribution on the crossed surface. It is a fact that a correct reconstruction is made possible only by the use of a diffuser with good Lambertian properties [1].

It is the main objective of the present work to investigate the optical behavior of Labsphere diffuse standards of different nominal reflectivity, in order to check how much these real diffusers deviate from the ideal Lambertian behavior. The optical characterizations were performed by using original methods and instrumentations. In particular, the total hemispherical reflectance was measured by a reflectometer, the CAR (Continuous Angle Reflectometer) apparatus, designed to vary the angle of incidence of a laser beam in a continuous way, at three different wavelengths in the visible and infrared spectrum. The optical characterizations of Labsphere samples were followed by SEM-EDS characterizations for investigating their morphological and structural properties.

2. The Diffuse Reflectance Standards

We investigated the set of Labsphere diffuse reflectance standards of the type Spectralon® [29]. They are durable,

* Corresponding author:
aparretta@alice.it (Antonio Parretta)
Published online at http://journal.sapub.org/optics

chemically inert standards with typical reflectance values ranging from 2% to 99% and are quite spectrally flat over the UV-VIS-NIR spectrum. All Spectralon materials are optically flat to +/- 4% over the range of 250÷2500 nm and +/- 1% over the photopic region of the spectrum.

Figure 1. The complete set of the SRS-xx-030 series samples

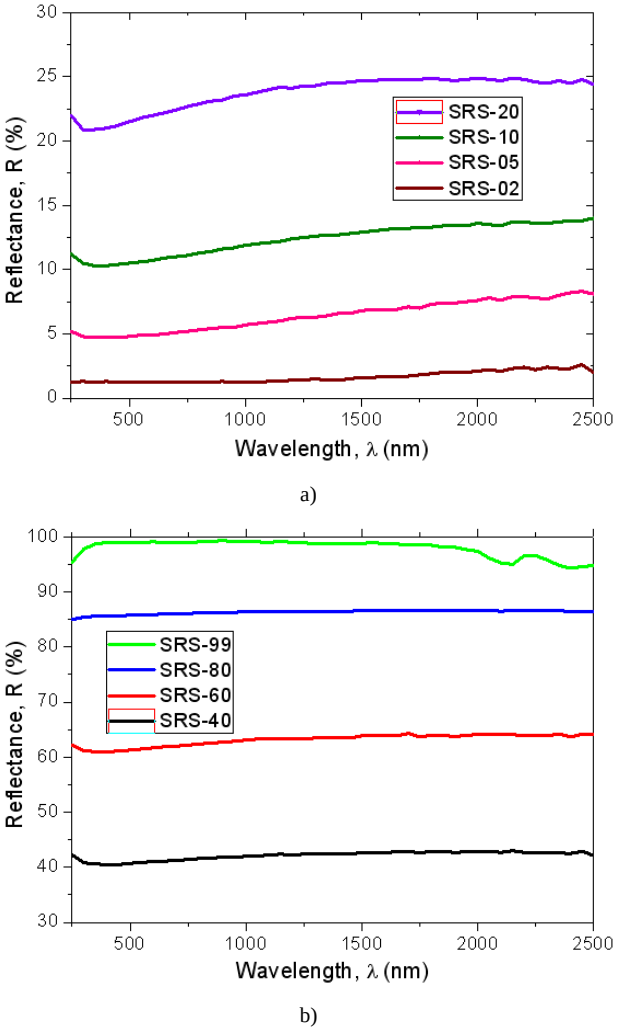

Figure 2. Total hemispherical spectral reflectance curves, at 8 ° incidence, in the 250÷2500 nm range, of the 2, 5, 10, 20% nominal reflectance standards (a), and of the 40, 60, 80, 99% nominal reflectance standards (b)

Labsphere declares that Spectralon Diffuse Reflectance Standards are highly Lambertian, with Spectralon SRM-99 reflectance material being the most Lambertian reflector available for use over the wavelength range 250÷2500 nm. The Spectralon diffuse reflectance standards were in a set consisting of a diffuse white standard and a selection of diffuse gray standards. The samples are composed of a polymer resin based on fluoropolymers, with high reflectivity. The mixture of this material with particles of carbon black, used as a black pigment, reduces the surface reflectivity in a controlled manner and then allows to obtain the series of standard samples characterized by a different nominal reflectance. The Spectralon reflectance standards are available in diameters of 1, 2 and 3 inches, and are identified as SRS-xx-yyy, where xx is the nominal percent reflectance, roughly corresponding to the average reflectance in the 250÷2500 nm spectral range, and yy.y is the diameter in inches. The standards that have the same nominal reflectance are exactly equal, regardless of the size; then, for the purposes of optical measurements, it is unconcerned the size of the standard. Fig. 1 shows a complete set of the 3 inches diameter set, SRS-xx-030, with xx = 02, 05, 10, 20, 40, 60, 80, 99. Each standard is supplied with a calibration certificate reporting the directional/hemispherical (d/h) reflectance data obtained at 8 ° incidence, in the 250÷2500 nm interval, and at 50 nm step. Fig. 2a shows the total hemispherical spectral reflectance curves for the four samples in the low reflectivity range (2%, 5%, 10%, 20%), whereas Fig. 2b shows the same quantity for the four samples in the high reflectivity range (40%, 60%, 80%, 99%).

3. Optical Characterization Methods

3.1. The CAR Reflectometer

Before describing the CAR reflectometer, it is useful to recall here that the first Lambert's law establishes that a Lambertian diffuser, when irradiated by a parallel beam, manifests a total reflectance constant with respect to the incidence angle [1]. This law can be stated in equivalent way saying that the flux reflected by the unit area varies as the cosine of the angle of incidence. For this reason, this law is also known as the first cosine law. The second cosine law regards the behavior of diffused light intensity and is discussed in Section 3.2.

The CAR apparatus was realized at the ENEA-Portici labs and is the evolution of the ROSE (Reflectometer for Optical measurements in Solar Energy) apparatus [4-9, 13, 18, 20], equipped with a series of windows to address the incident beam towards the sample at variable angles with 10 ° steps. Unlike ROSE, the CAR reflectometer was designed to vary continuously the angle of incidence of the beam. For this purpose, the integrating sphere of the CAR, of 40-cm diameter as that of ROSE, was designed with a slit (sl), 1-cm wide, that extends to a 180 ° arc onto the equatorial plane and works as input port for the laser beam. The CAR apparatus is schematically shown in Fig. 3 and illustrated in

the photos of Fig. 4. In the following, we describe the measure on a generic Labsphere standard as if it were a test sample (sa) to be compared to a reference standard (ref), eventually coincident with the test sample itself.

Three different types of laser sources (la) were used: a He-Ne laser Melles-Griot of ~10 mW operating at λ = 543 nm (green), a He-Ne laser Lot-Oriel of ~25 mW operating at λ = 633 nm (red), and a diode-pumped solid state laser BWR-50 of BWTEK, of ~50 mW, operating at λ = 1064 nm (NIR). All the lasers were unpolarized and operating in CW mode. The laser beam crosses at first the neutral filter (fi), then the diaphragm (di) and is mechanically modulated by the "chopper" (ch), that provides the reference signal for the lock-in amplifiers (li1) and (li2). The chopped laser beam is then sent to the beam splitter (bs), where its intensity is monitored by the photodetector (r1) connected to the lock-in amplifier (li1). The laser beam transmitted by the (bs) crosses the second diaphragm (di), enters the integrating sphere (is) through the slit (sl) and strikes the sample (sa) or the reference standard (ref) faced to window (ws).

The total radiation reflected by the test sample is collected and integrated by the integrating sphere (is), then is measured by a second photodetector (r2) connected to the lock-in amplifier (li2). The lock-in amplifiers (li1) and (li2) selectively amplifies the signals modulated at the frequency of the chopper (ch).

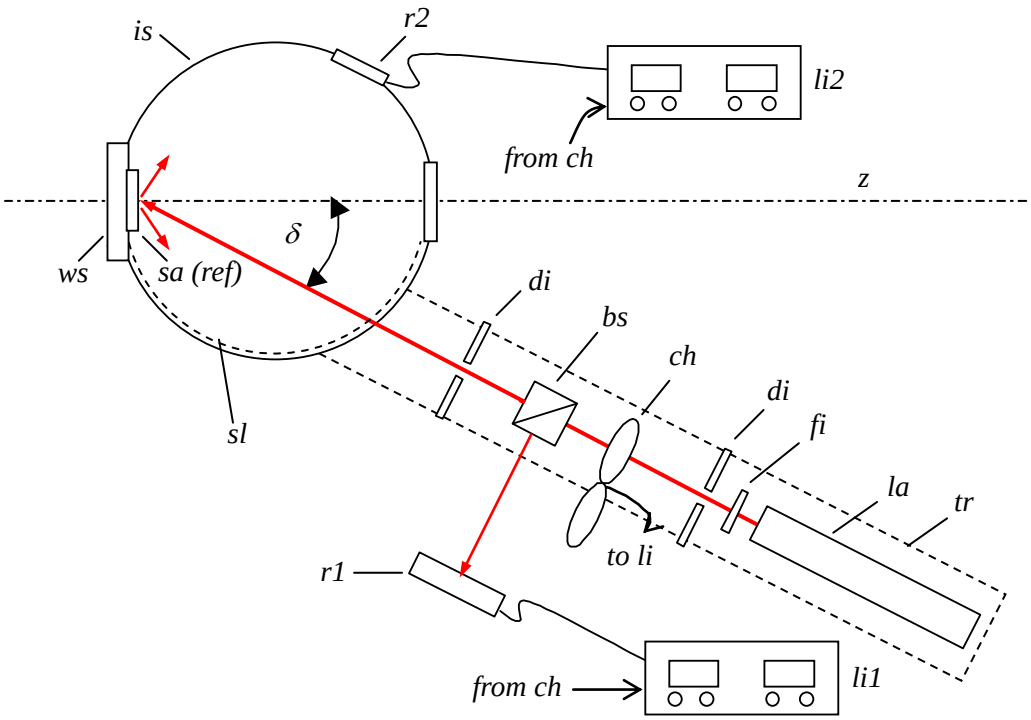

Figure 3. Schematic top view of the CAR apparatus

a) b)

Figure 4. Overall view (a) and details (b) of the CAR apparatus

Thanks to the innovative design of the CAR sphere, it was possible to vary the angle of incidence of the laser beam on the test sample with continuity between ~10 ° and ~80 °. To move the laser source (la) respect to the sphere (is), the laser source and its accessories were assembled together on a track (tr), which is rotated by angle δ around the vertical axis crossing the center of the sample (sa). The calibration measurements can be carried out in two alternative ways: i) by removing sample (sa), a Labsphere standard, and replacing it with another Labsphere standard taken as reference (ref), irradiating this one at 8 ° and measuring the corresponding signal to be assigned to the spectral reflectance reported on the calibration chart (see Fig. 2); ii) by keeping the sample (sa), a Labsphere standard, on window (ws) and simply redirecting the laser beam in order to irradiate it at 8 °, in this way using the same sample (sa) as the reference standard (ref) for calibration, of known reflectance at 8 °, as obtained by the calibration chart.

3.2. The Optical Scatterometer

The second Lambert's law establishes for a Lambertian diffuser a reflected light with constant radiance $L(\theta)$ (W/sr m^2) as function of the polar scattering angle θ; this is equivalent to say that the radiant intensity $I(\theta)$ (W/sr) must follow a $\cos\theta$ behavior. For this reason, this law is also known as the second cosine law [1]. The angular distribution of scattered light has been investigated on the plane of incidence of the laser beam.

In this way, it is represented by a curve, the "reflectance indicatrix" [1], which describes the variation, with the observation, or scattering angle of the radiant intensity of light, $I(\theta)$. For a Lambertian diffuser the indicatrix (in) is a circle that we have drawn tangent to the test surface in Fig. 5. For measuring the indicatrix, it was set up the scatterometer schematically shown in Fig. 5 and illustrated in the photos of Fig. 6. In the same way as for the CAR, the collimated and unpolarized beam from the laser source (la), spatially selected by the diaphragm (di), is mechanically modulated by chopper (ch), monitored by detector (r1) and lock-in amplifier (li1), after being splitted at beam splitter (bs) and attenuated by the neutral filter (fi); finally it crosses a second diaphragm (di) and strikes the sample (sa) at the incidence angle δ. The radiant intensity is measured rotating detector (r2) around the sample (sa), keeping it oriented towards (sa) and at a constant distance. As the solid angle of collected light is constant, the photocurrent from (r2) is proportional to the radiant intensity $I(\theta)$. The scattering angle θ is varied from -90 ° to +90 °, being the indicatrix curve not generally symmetric respect to $\tilde{n}$, the normal to sample surface. The polarization degree of light diffused along direction θ is obtained by placing a polarizer (po) in front of (r2) and taking several measures of intensity to draw the polarization ellipse. The polarization degree is reported in terms of inverse ellipticity. As for the CAR apparatus, the signal from (r2) and (li2) is normalized to the signal from (r1).

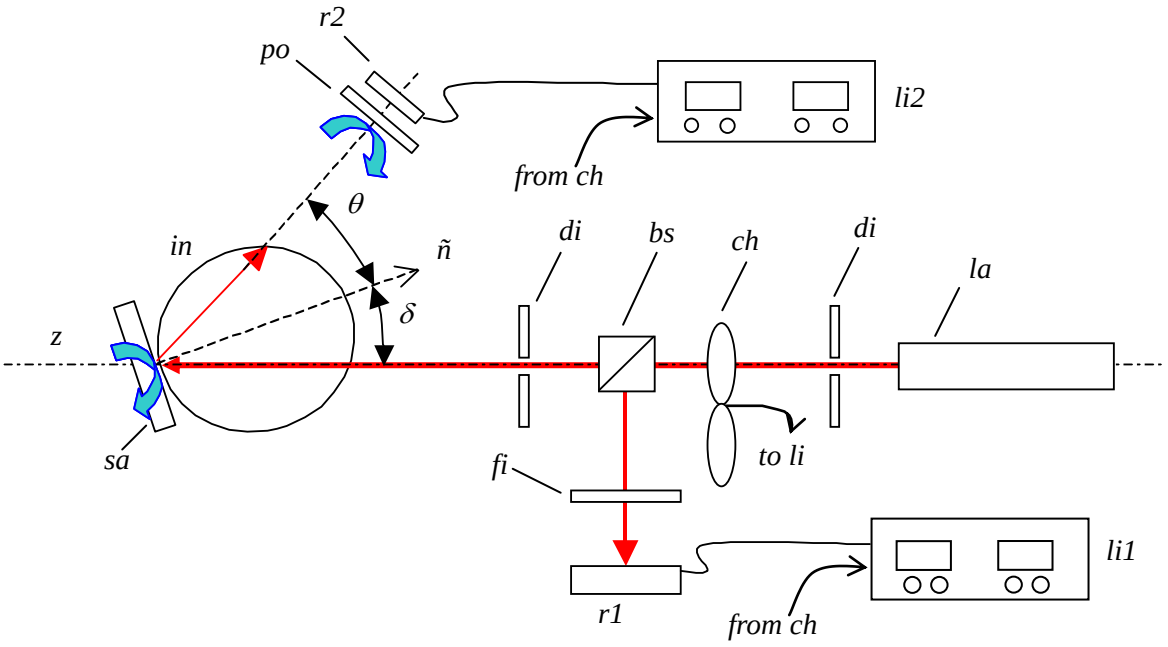

Figure 5. Scheme of the apparatus for the measurement of angular distribution of intensity and polarization of scattered light

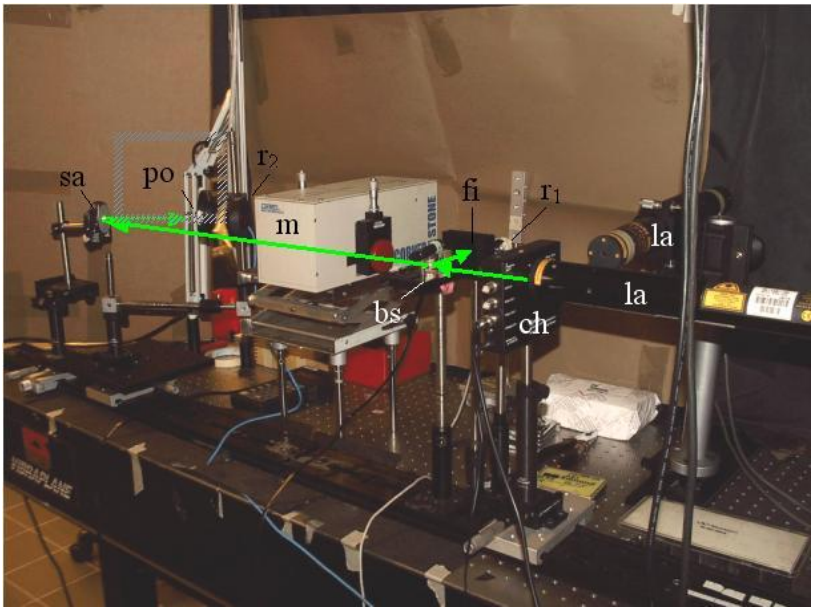

(a)

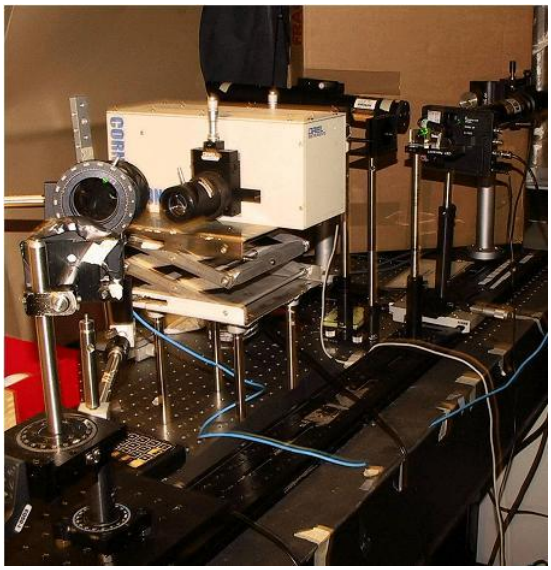

(b)

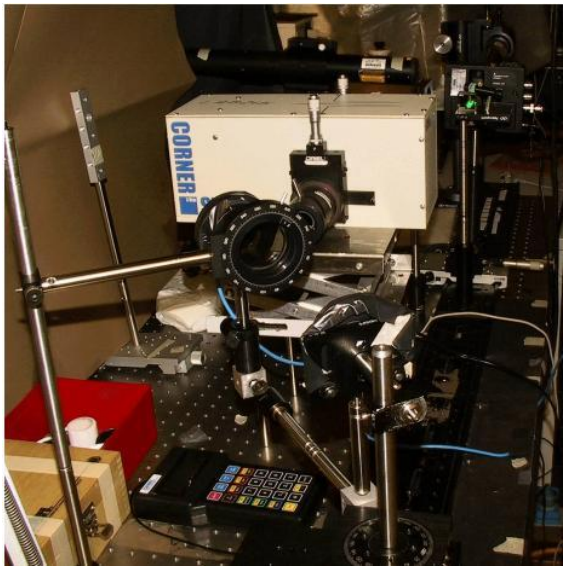

(c)

Figure 6. Photos of the apparatus for measurement of the angular distribution of intensity and polarization of light scattered by the sample (sa). In (a) it is shown the path of a ray of green light (λ = 543 nm). The laser of red light is also shown. In (b) and (c) photos of other details of the scatterometer

4. Theoretical Aspects of Reflectance Measurements

The theory of reflectance measurements by the CAR apparatus is derived by that of an integrating sphere [30-34]. The formula for the correct value of reflectance is derived by the expression of the stationary irradiance incident on the sphere wall. We briefly outline here the procedure for obtaining the stationary irradiance in the simple case of an integrating sphere, of radius *r*, of homogeneous wall reflectivity ρ_w, and provided with a series of *N* openings, or ports, with zero reflectivity and relative area f_i (see Fig. 7).

If we irradiate the sphere with a collimated beam of flux Φ_{in}, impinging on the sphere wall, we have that the reflectivity of the first impact surface is: $\rho_{first} = \rho_w$. The first reflected flux is therefore:

$$\Phi_R(1) = \rho_{first} \cdot \Phi_{in} \qquad (1)$$

As the integrating sphere has a wall with Lambertian properties, this flux diffuses inside the sphere with uniform radiance, producing an irradiance $E_w(1)$ given by:

$$E_w(1) = \Phi_R(1) / A_{sph} = \Phi_R(1) / (4\pi \cdot r^2) \qquad (2)$$

where A_{sph} is the total area of the sphere. The irradiance

$E_w(1)$ produces a second reflected flux given by:

$$\Phi_R(2) = E_w(1) \cdot \rho_w \cdot A_{sph} \cdot (1 - \sum_{i=1}^{N} f_i) \quad (3)$$

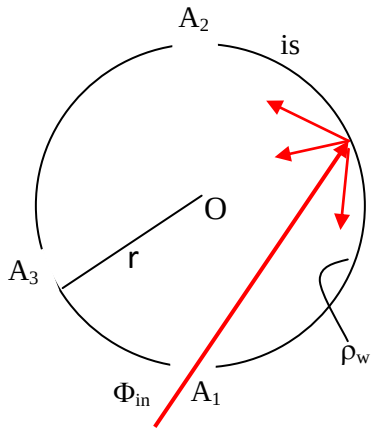

Figure 7. Schematic representation of a simple integrating sphere, of *r* diameter and ρ_w wall reflectivity, provided with three open ports

The irradiance corresponding to this flux, $E_w(2)$, is a contribution that adds to $E_w(1)$ and is given by:

$$E_w(2) = \Phi_R(2) / A_{sph} = E_w(1) \cdot \rho_w \cdot (1 - \sum_{i=1}^{N} f_i) \quad (4)$$

Proceeding in this way, we have for the n-th contribution to wall irradiance:

$$E_w(n) = \Phi_R(n) / A_{sph} = E_w(1) \cdot (\rho_w)^{n-1} \cdot (1 - \sum_{i=1}^{N} f_i)^{n-1} \quad (5)$$

The stationary irradiance on the wall, after an infinite number of reflections, is given by:

$$E_w = \sum_{n=1}^{\infty} E_w(1) \cdot (\rho_w)^{n-1} \cdot (1 - \sum_{i=1}^{N} f_i)^{n-1} = \ldots$$
$$\ldots = E_w(1) \cdot \sum_{n=1}^{\infty} (\rho_w)^{n-1} \cdot (1 - \sum_{i=1}^{N} f_i)^{n-1} \quad (6)$$

It is easy to find that, being ρ_w<1 and $(1 - \sum_{i=1}^{N} f_i)$ <1, the final expression for E_w becomes:

$$E_w = E_w(1) \cdot \frac{1}{1 - \rho_w \cdot (1 - \sum_{i=1}^{N} f_i)} = \ldots$$
$$\ldots = \frac{\rho_{first} \cdot \Phi_{in}}{A_{sph}} \cdot \frac{1}{1 - \rho_w \cdot (1 - \sum_{i=1}^{N} f_i)} \quad (7)$$

The expression (7) of irradiance incident on the wall can be immediately extended to a sphere with a series of *N* openings characterized by reflectivity ρ_i:

$$E_w = \frac{\rho_{first} \cdot \Phi_{in}}{A_{sph}} \cdot \frac{1}{1 - \rho_w \cdot (1 - \sum_{i=1}^{N} f_i) - \sum_{i=1}^{N} \rho_i \cdot f_i} \quad (8)$$

So far we have not considered the dependence of the introduced quantities on the wavelength of light; this dependence, however, must be considered and included in the above equations.

The irradiance E_w induces a proportional current signal *S* on the photodetector (r2) (see Fig. 3), that is measured by the lock-in amplifier (li2) and normalized to the signal on (r1). The sphere of the CAR in the configuration of Fig. 3, for example, can be modeled as provided with a port for the sample (sa) (i=1), a port for the photodetector (r2) (i=2) and an opening for the slit (sl) (i=3). The measure of reflectance is carried out in the following way: i) the sample under test (sa), of reflectivity ρ_X, is placed at the sample port (ws) (i=1); ii) the signal S_X from (r2) is measured by the lock-in amplifier (li2); iii) a "reference" standard of reflectance (ref), of reflectivity ρ_{REF}, is placed at the sample port (ws) (i=1) in place of the test sample (sa); iv) the signal S_{REF} from (r2) is measured by the lock-in amplifier (li2). Then we have, when measuring the test sample: $\rho_{first} = \rho_1 = \rho_X$, whereas, when measuring the reference standard of reflectance: $\rho_{first} = \rho_1 = \rho_{REF}$. In both cases we have: $\rho_3 = 0$, because the slit behaves as an open port.

By applying Eq. (8) to the case of test sample, we have:

$$E_w(X) = \frac{\rho_X \cdot \Phi_{in}}{A_{sph}} \cdot \frac{1}{1 - \rho_w \cdot (1 - \Sigma_1) - \Sigma_2(X)} \quad (9)$$

where: $\Sigma_1 = f_1 + f_2 + f_3$ is a constant and known quantity, $\Sigma_2(X) = \rho_X \cdot f_1 + \rho_2 \cdot f_2$ is an unknown quantity. By applying Eq. (8) to the case of the reference standard, we have:

$$E_w(REF) = \frac{\rho_{REF} \cdot \Phi_{in}}{A_{sph}} \cdot \frac{1}{1 - \rho_w \cdot (1 - \Sigma_1) - \Sigma_2(REF)} \quad (10)$$

where: $\Sigma_2(REF) = \rho_{REF} \cdot f_1 + \rho_2 \cdot f_2$ is a known quantity.

As the photodetectors (r1) and (r2) operate in a linear regime, the signals to the lock-in amplifier, corresponding to the test sample and to the standard, become, respectively, $S(X) = k \cdot E_w(X)$ and $S(REF) = k \cdot E_w(REF)$.

By calling *R* the ratio between the two measurements, we

have:

$$R = \frac{S(X)}{S(REF)} = \frac{E_w(X)}{E_w(REF)} = \ldots$$
$$\ldots = \frac{\rho_X}{\rho_{REF}} \cdot \frac{1-\rho_w \cdot (1-\Sigma_1) - \Sigma_2(REF)}{1-\rho_w \cdot (1-\Sigma_1) - \Sigma_2(X)} \quad (11)$$

From which we obtain:

$$\rho_X = \frac{R \cdot \rho_{REF} \cdot [1-\rho_w \cdot (1-\Sigma_1) - \rho_2 \cdot f_2]}{R \cdot \rho_{REF} \cdot f_1 + 1 - \rho_w \cdot (1-\Sigma_1) - \Sigma_2(REF)} \quad (12a)$$

Eq. (12a) gives the final, correct formula for the calculation of ρ_X. In some cases, however, the long formula (12a) is not required. This is true whenever the area of the sample port is negligible respect to the sphere area A_{sph}, or when the reflectance of the standard is similar to that of the test sample. This will be clear writing Eq. (12a) in the following way:

$$\rho_X = \frac{R \cdot \rho_{REF} \cdot [1-\rho_w \cdot (1-\Sigma_1) - \rho_2 \cdot f_2]}{\rho_{REF} \cdot f_1 \cdot (R-1) + [1-\rho_w \cdot (1-\Sigma_1) - \rho_2 \cdot f_2]}$$
$$\ldots = \frac{R \cdot \rho_{REF}}{1 + \frac{\rho_{REF} \cdot f_1 \cdot (R-1)}{[1-\rho_w \cdot (1-\Sigma_1) - \rho_2 \cdot f_2]}} \quad (12b)$$

From Eq. (12b) we see that, if $R \approx 1$, that is the standard has a reflectance similar to that of the test sample, or if the fraction area of the test sample is very little ($f_1 \approx 0$), in both cases we have that the second addendum of the denominator vanishes and then the expression for the unknown reflectivity ρ_X reduces to:

$$\rho_X = R \cdot \rho_{REF} \quad (13)$$

that is the common formula used for fast, approximated reflectance measurements.

5. Results and Discussion

5.1. Total Hemispherical Reflectance

The angle-resolved total directional / hemispherical reflectance, $R_{dh}(\delta)$, was measured on a complete set of Labsphere Spectralon samples of 3-inches diameter: SRS-02-030 (2%), SRS-05-030 (5%), SRS-10-030 (10%), SRS-20-030 (20%), SRS-40-030 (40%), SRS-60-030 (60%), SRS-80-030 (80%) and SRS-99-030 (99%) (the nominal reflectance is in parentheses). Measurements were carried out at three wavelengths: 543 nm (green), 633 nm (red), 1064 nm (NIR), and the results are reported in Figs. 8 (a-c), respectively. Remembering that "Lambertianity" requires a constant reflectance vs. the incidence angle [1], we observe that most of the samples show quite good characteristics of Lambertianity, as declared by Labsphere; however, this condition is better respected here by the samples with high nominal reflectance. The reflectance curves at the three different wavelengths for the standards with 40%, 60%, 80% and 99% nominal reflectance are compared in Fig. 9.

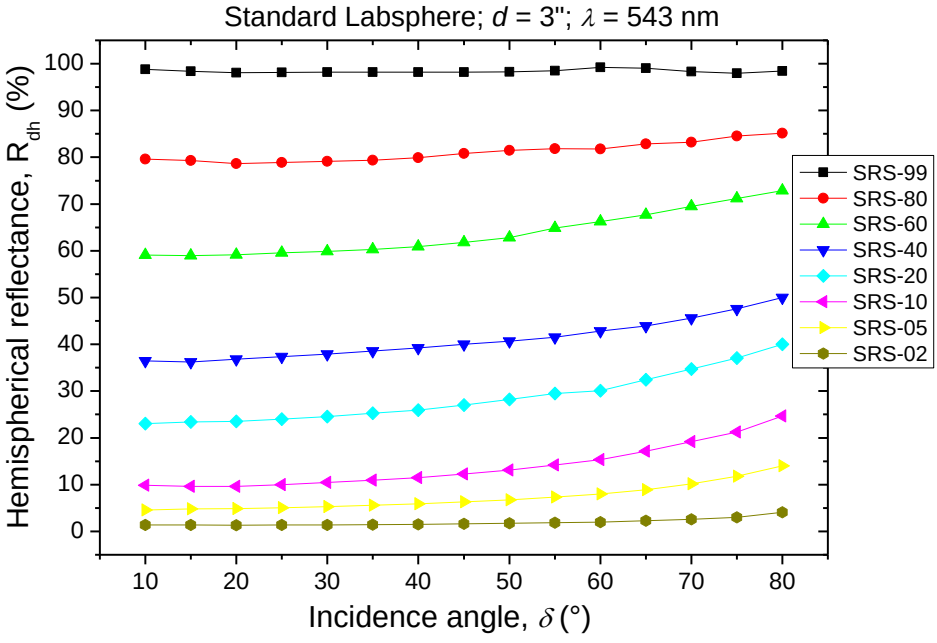

a)

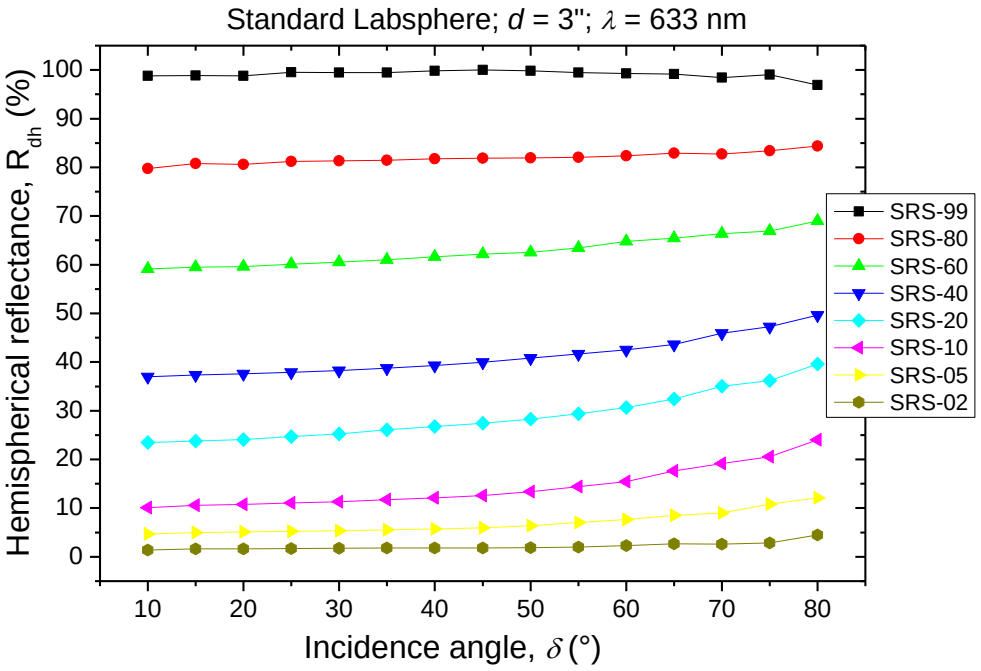

b)

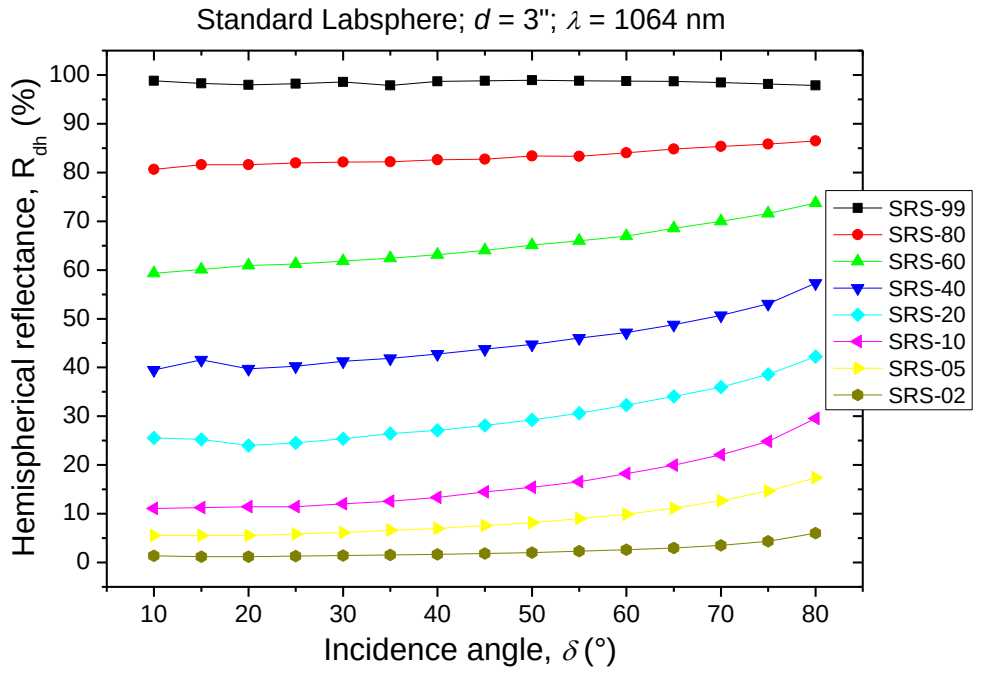

c)

Figure 8. Total hemispherical reflectance vs. the angle of incidence (δ) for the set of 3-inches Labsphere Spectralon standard samples: (a) λ = 543 nm; (b) λ = 633 nm; (a) λ = 1064 nm

The increase of total reflectance at increasing δ can be explained considering that the increase of δ reduces the absorption depth of radiation; this has the effect to reduce the chance for the radiation to be randomized and favors the appearance of a "specular" component, generally a "hump", which is less absorbed by the material and finally determines an increase of total reflectance. To have a rough estimate of the deviation from ideality of the various standards, we have calculated the relative increase of total reflectance, ΔR_{tot} (%), when moving from δ = 10 ° to δ = 40 ° (see Fig. 10).

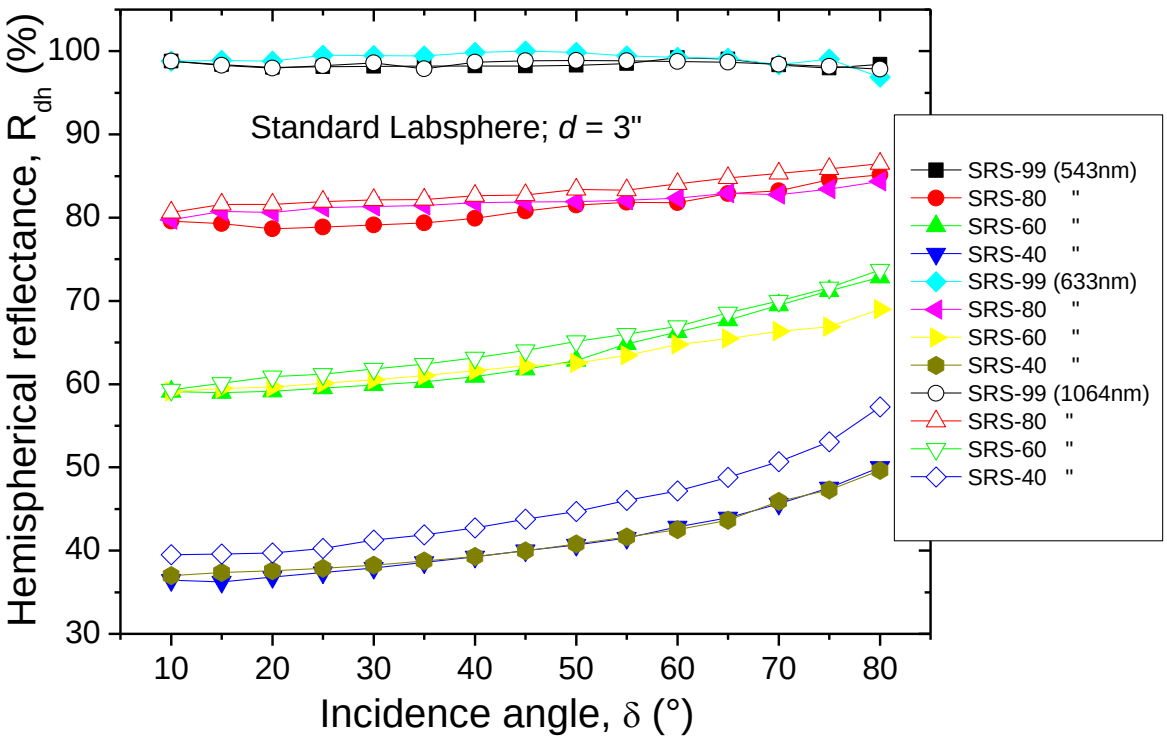

Figure 9. Comparison of reflectance curves obtained at 543 nm, 633 nm and 1064, for the 3-inches Labsphere standards of higher nominal reflectance (40%, 60%, 80%, 99%)

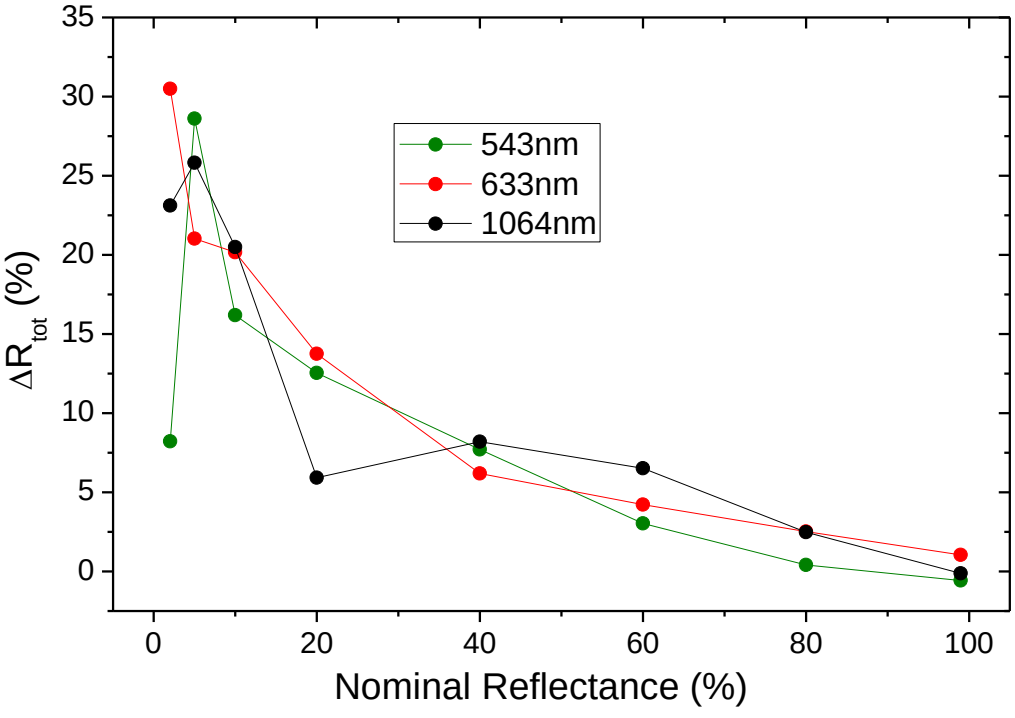

Figure 10. Relative increase of total reflectance moving the incidence angle from $\delta = 10°$ to $\delta = 40°$, calculated at wavelengths: λ = 543, 633 and 1064 nm

We observe that ΔR_{tot} increases monotonically at decreasing the nominal reflectance, with one exception for the SRS-02 standard at λ = 543 nm; the same standard shows an abnormal behavior of the diffused light intensity distribution, as it will be shown in Section 5.2. For the SRS-99, SRS-80, SRS-60 and SRS-40 standards, the relative increase of total reflectance remains below 10%. These four samples are also those better respecting the second Lambert's cosine law, as we shall see by analyzing the angular distribution of scattered light intensity (Section 5.2).

5.2. Analysis of the Scattered Light Intensity

The angular distribution of the intensity of scattered light (radiant intensity) was measured at λ =543 nm on the samples SRS-02-020, SRS-10-020, SRS-40-020, SRS-60-020, SRS-80-020 and SRS-99-020, choosing, for the angle of incidence, the values: δ = 0 °, 10 °, 20 °, 30 ° and 40 °. The results are reported in Figs. 11(a-e), together with the curve of cosθ, which represents the behavior of a Lambertian diffuser (as discussed in Section 3.2), to show how much the experimental curves deviate from the ideal behavior. In the figures, the negative angles are angles measured from the incident beam side, and then are affected by a shadow zone produced by the photodetector, while the positive ones represent the angles measured from the side of the "specular" beam, imagining the sample like a mirror.

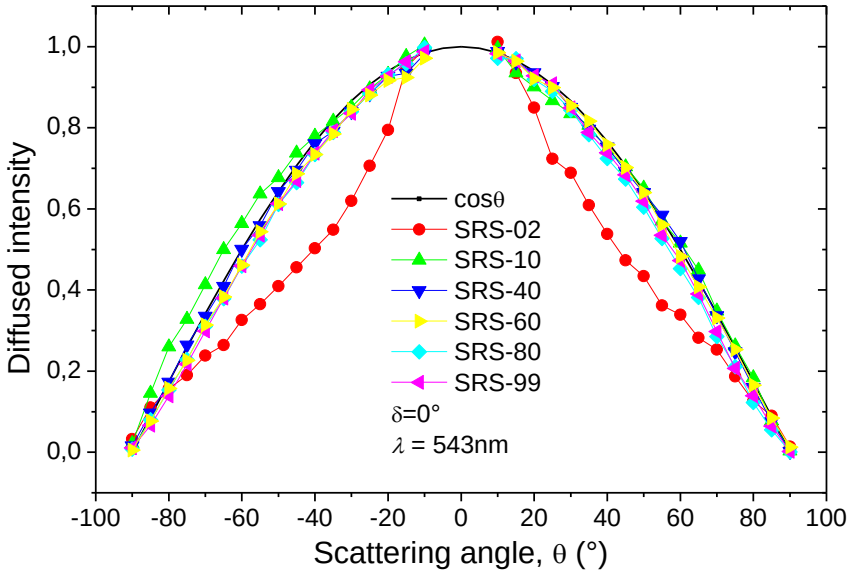

a)

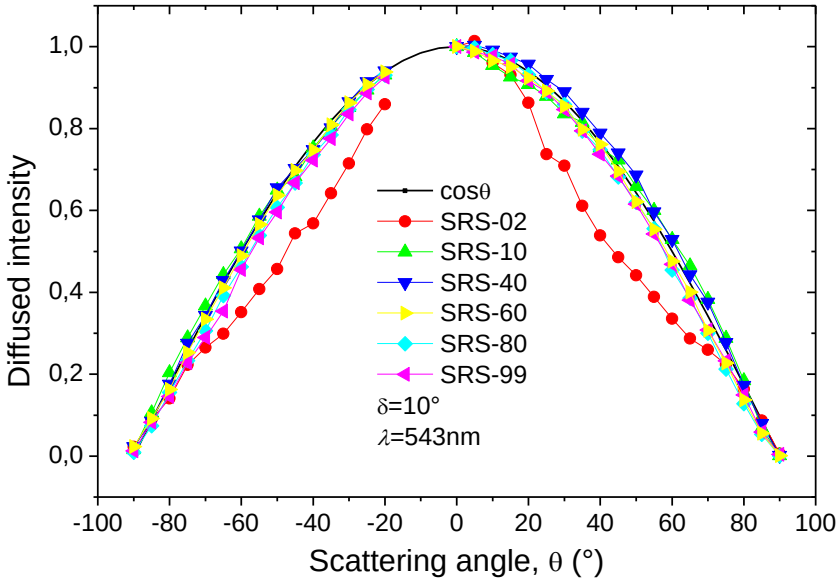

b)

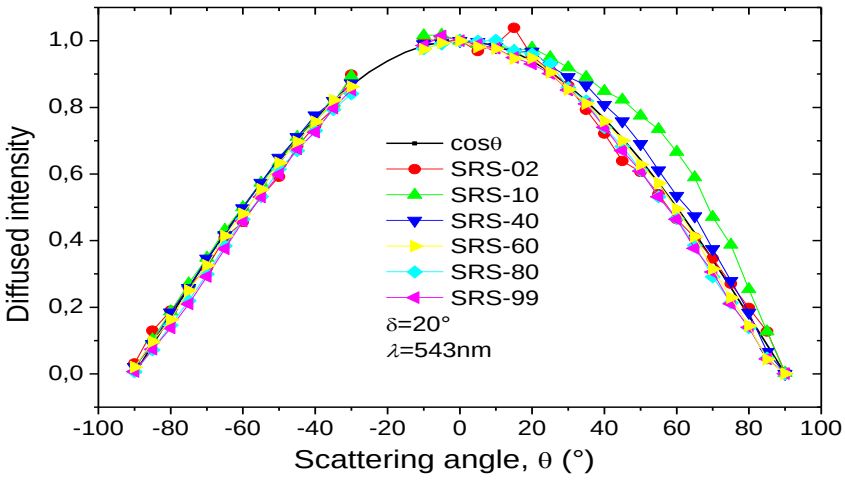

c)

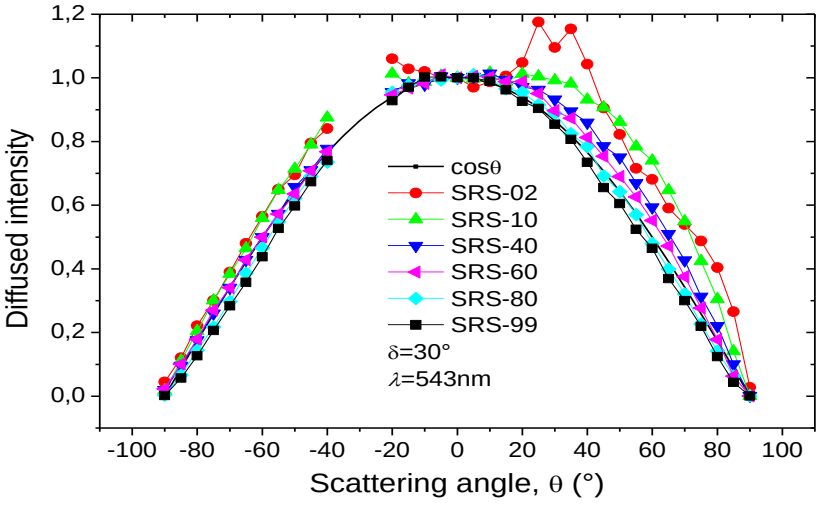

d)

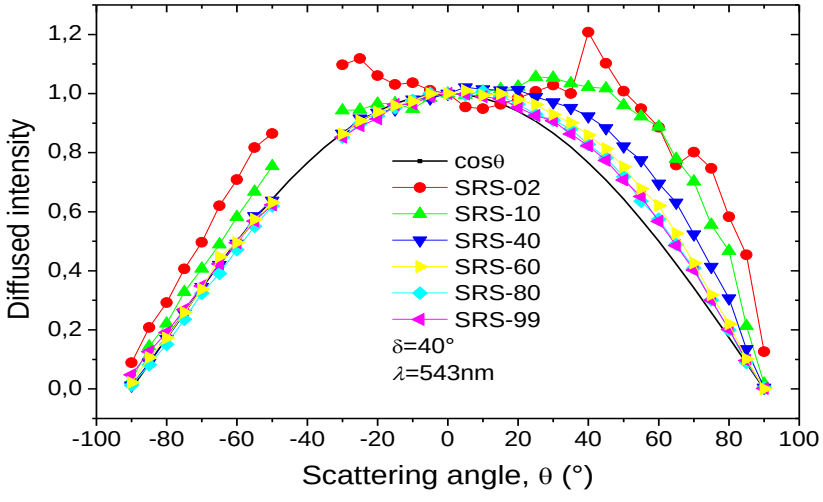

e)

Figure 11. Relative radiant intensity curves of some Spectralon standards SRS-xx-020 vs. the scattering angle θ, obtained at λ = 543 nm and at incidence angles: (a) δ = 0 °; (b) δ = 10 °; (c) δ = 20 °; (d) δ = 30 °; (e) δ = 40 °

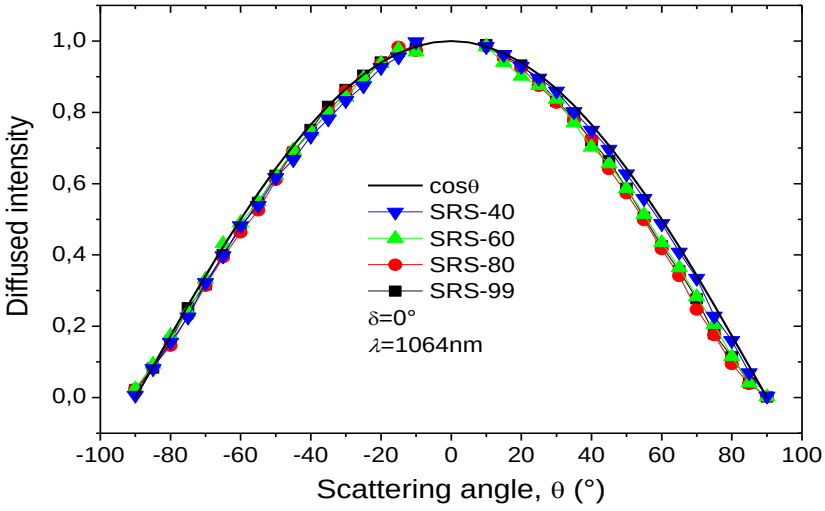

a)

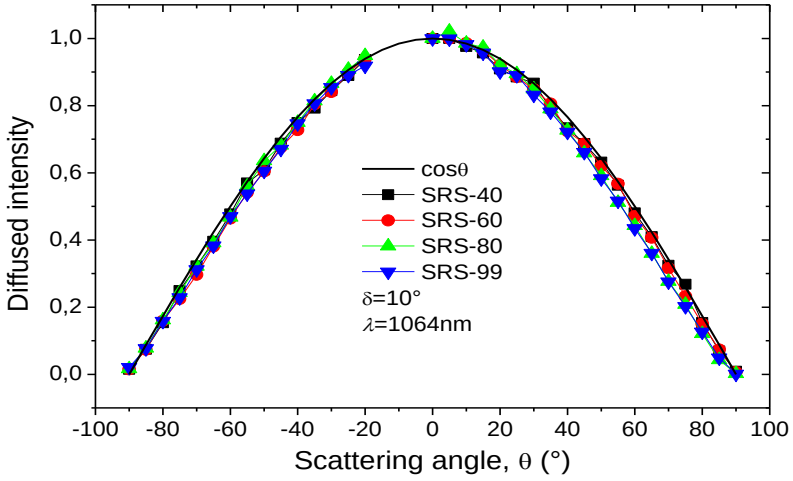

b)

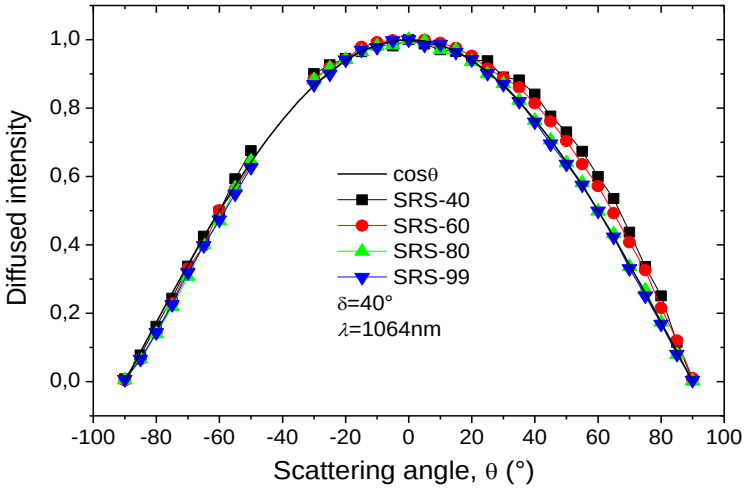

c)

Figure 12. Relative radiant intensity curves of the Spectralon standards SRS-40-020, SRS-60-020, SRS-80-020 and SRS-99-020, vs. the scattering angle θ, obtained at λ = 1064 nm at incidence angles: (a) δ = 0 °; (b) δ = 10 °; (c) δ = 40 °

All curves of relative radiant intensity were normalized setting equal to one the radiant intensity measured at 0 ° scattering. In reality, the curves corresponding to higher incidence angles are slightly more intense (see Fig. 8). As it can be seen in Fig. 11a (angle $\delta = 0$ °), all the samples, except the SRS-02 one, the darkest, show an almost Lambertian behavior; more precisely we note that samples from 40% to 99% reflectance show an excellent Lambertian behavior. The 2% reflectance sample instead has a strong specular character, because the radiant intensity shows a large band occurring at an angle of diffusion of 0 °, the same of the incidence angle. At angle of incidence $\delta = 10$ ° (Fig. 11b), the situation improves because all samples from 10% to 99% can be considered excellent Lambertian, but the 2% sample remains yet far from ideality, as for $\delta = 0$ °.

The situation changes unexpectedly at the incidence angle $\delta = 20$ ° (Fig. 11c) for the 2% sample, which turns into a Lambertian diffuser. At the same time, the sample of 10% reflectance moves out from ideality showing a forward scattering hump, i.e. an enhanced reflection in the opposite direction to that of the light source. The other samples remain Lambertian. At $\delta = 30$ ° incidence (Fig. 11d), some samples show the appearance of a small forward scattering hump and the 2% reflectance sample shows a little specular reflection. At this angle of incidence, the 2% and 10% samples begin to show a back hump, i.e. a back reflection towards the light source. The $\delta = 40$ ° incidence angle (Fig. 11e) moves almost all samples far from ideality, although to varying degrees, higher for lower reflectance standards. The samples that can still be considered fully Lambertian are the 80% and 99% ones, to a lesser extent the 60% one. The choice of the suitable reflectance standards, to be used as Lambertian diffusers with the various optical characterization apparatus, depends therefore on the maximum divergence angle of the incident beam. If the angle of incidence is limited to 30 °, the diffusers with a very good Lambertian character are: 40%, 60%, 80% and 99%; if the maximum angle of incidence is instead 40 °, the diffusers with very good Lambertian character are the 60%, 80% and 99% ones.

Some light diffused intensity measurements were made also in the NIR at $\lambda = 1064$ nm. The results are reported in Figs. 12(a-c). At this wavelength, the four samples selected after the first set of measurements at $\lambda = 543$ nm (SRS-40, SRS-60, SRS-80 and SRS-99) all behave very close to the ideal, that is they approach very well the $\cos\theta$ function. From the curves of Figs. 12(a-c) we observe in fact only a very small hump at $\delta = 40$ °. It is likely that the greater penetration depth into the material of NIR radiation than that of visible radiation causes it to be more easily randomized inside the porous material and then to escape with a widespread distribution of Lambertian character.

From the curves of Fig. 12, as consequence of what said, we note the complete absence of forward or backward reflective characteristics. This aspect will be discussed in the next section, devoted to the morphological and structural characterizations at SEM-EDS.

5.3. Analysis of the Scattered Light Polarization

The polarization of the scattered light was analyzed for the Labsphere samples of the SRS-xx-020 series, that is of 2-inches diameter, and at the wavelength $\lambda = 543$ nm. The degree of polarization is normally expressed in terms of "ellipticity", defined as the ratio b/a between the major and the minor axis of the polarization ellipse. Here we use the quantity "inverse ellipticity" a/b in order to have always values smaller than one ($a/b = 0$: maximum polarization; $a/b = 1$: absence of polarization). In Fig. 13 it is shown, by way of example, the polarization ellipse measured for the SRS-02-020 standard at an angle of observation $\theta = 50$ °. The inverse ellipticity, a/b, measured on some samples of the series SRS-xx-020 at an angle of incidence $\delta = 0$ °, is reported in Fig. 14. This figure shows that only the less reflective samples, SRS-02, SRS-05 and SRS-10, cause a polarization in the diffused light. The SRS-02 sample induces a strong polarization on the diffused light; less polarization is induced by the SRS-05 and SRS-10 samples. The inverse ellipticity tends to decrease at increasing the scattering angle, then the polarization tends to increase at increasing the scattering angle. This is particularly evident for the SRS-02 sample.

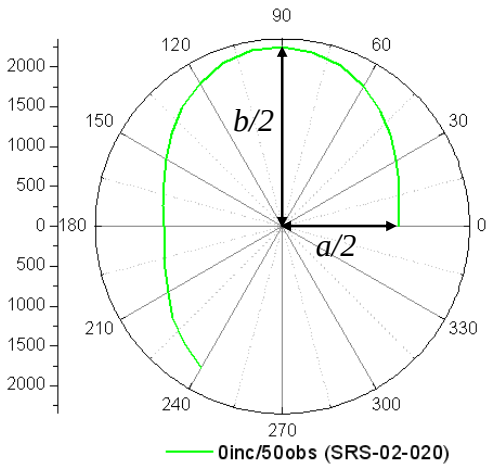

Figure 13. Polarization ellipse of diffused light ($\lambda = 543$ nm) measured for the SRS-02 standard at incidence angle $\delta = 0$ ° and observation angle $\theta = 50$ °

The Labsphere samples that showed a nearly Lambertian behavior were the samples SRS-40/60/80/99; they indeed induce no appreciable polarization of diffused light up to scattering angles of 75 °.

5.4. Morphological and Structural Characterization

The characterization of surface morphology and internal structure of diffuse reflectance standards Labsphere was made by scanning electron microscopy (SEM), and the compositional analysis, to identify the elemental constituents of the material used, was made by x-ray microanalysis (EDS). The measurements were performed on the samples SRS-02-020, SRS-40-020 and SRS-99-020 (2%, 40% and 99% of nominal reflectance, respectively). The surface morphology of the three samples is shown in Figs. 15 (a-c). The surface is in all cases extremely wrinkled. In the sample

SRS-02 it looks like a conglomerate of rounded grains of varying sizes (from a few micrometers to a few tens of micrometers), while the standards with higher reflectivity are characterized by roughness of fractal type, accentuated in the sample of highest reflectivity. All specimens show a high internal porosity.

Higher magnification observations on samples of 2% and 99% reflectivity show a compact amorphous structure, connected by fibrous material (Fig. 16).

In the sample of 2% reflectivity we observe, mixed to the fibrous amorphous structure, spherical particles of sizes between 500 and 800 Å, due to the carbon black used as a black pigment to reduce the reflectivity of the material (Fig. 16a).

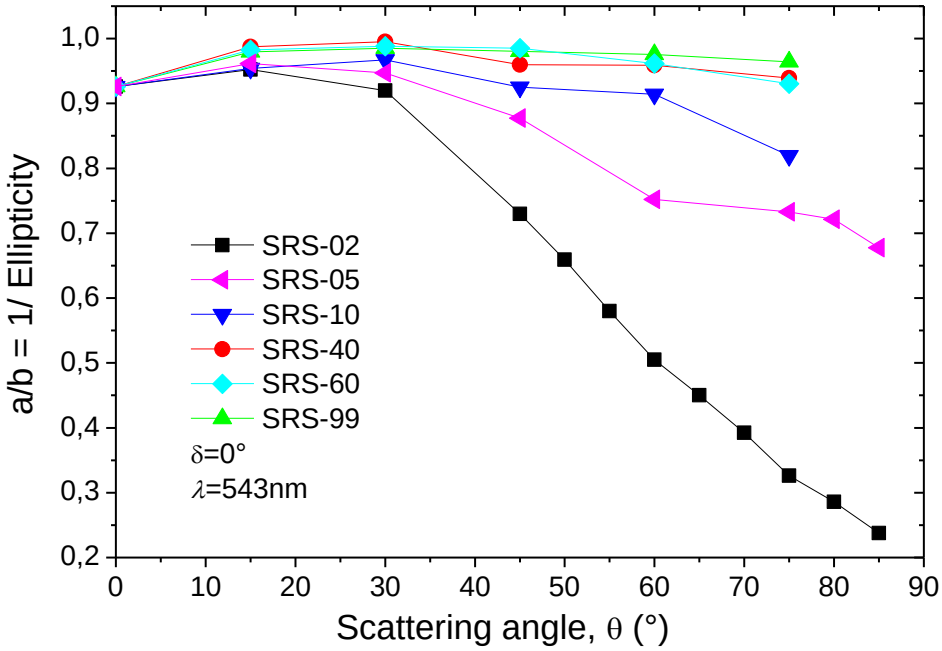

Figure 14. Inverse ellipticity of the light scattered by some samples of the SRS-xx-020 series, measured as function of the observation angle, at incidence of $\delta = 0°$ and at $\lambda = 543$ nm

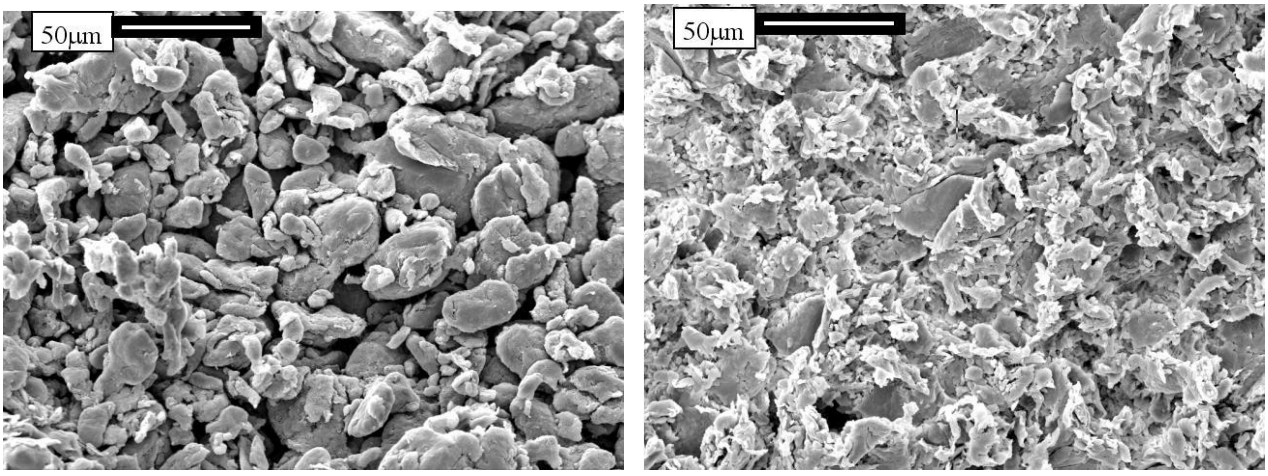

a) b)

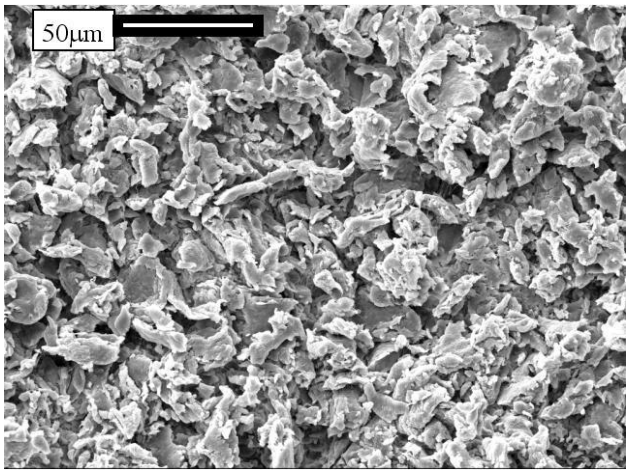

c)

Figure 15. SEM images of surface morphology of (a) SRS-02, (b) SRS-40 and (c) SRS-99 samples

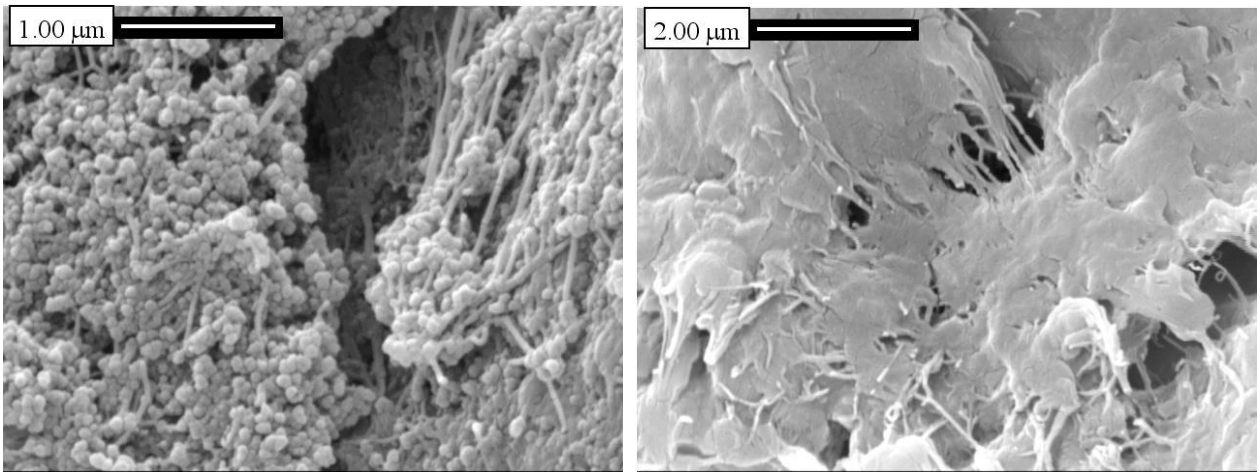

a) b)

Figure 16. High magnification SEM images of the structure of samples: (a) SRS-02 and (b) SRS-99

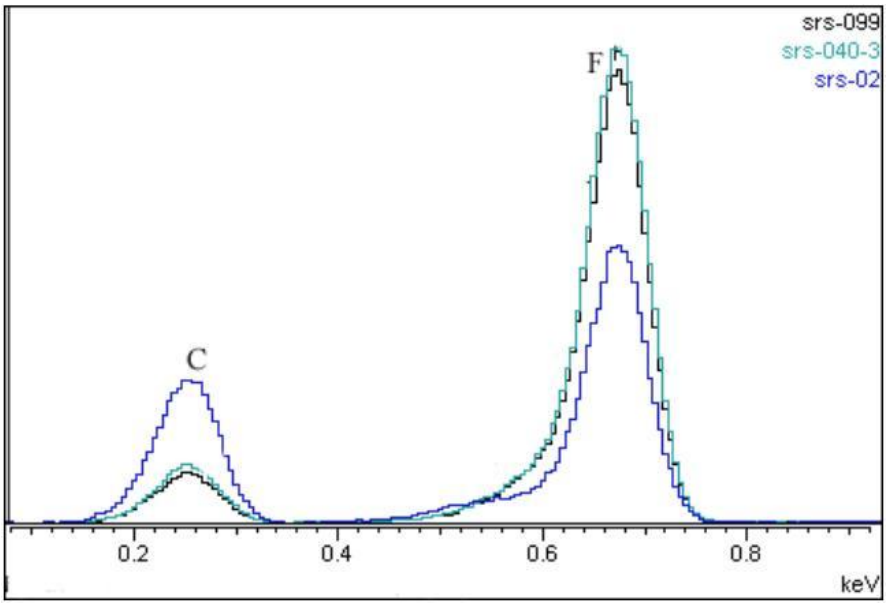

Figure 17. EDS spectra of the three Labsphere standards

The results of compositional measurements performed on the three samples are shown in the spectra of Fig. 17.

The qualitative analysis of the spectra shows the presence of fluorine and carbon in the SRS-40 and SRS-99 samples, while traces of oxygen are present in the SRS-02 sample. In the SRS-40 sample there is a little more quantity of carbon respect to the SRS-99 sample; instead, in the sample SRS-02 there is a notable increase in the amount of carbon due to the large amount of carbon black introduced as black pigment. The EDS analysis confirms the Labsphere standards composition as polymer resin based on fluoropolymers added to a variable quantity of carbon black.

We can now briefly discuss the correlation between optical and morphological-structural properties of the Labsphere standards. First of all, the morphological analysis at SEM on the three samples reveals that the surface roughness is much greater than the wavelength of light. This should result, in principle, in efficient light trapping for all the samples, independent on wavelength. The difference found on the optical properties of samples must be then justified only by a more accurate analysis of the morphology. In the SRS-99 sample the light trapping is always effective at any incidence angle, as the surface roughness is very evident and the porous network affecting the structure of surface and adjacent sub-surface area seems suitable to induce multiple reflections of light. In the SRS-40 sample the surface roughness has undergone a slight smoothing, due to the adding of small quantities of carbon black. This explains the appearance of the specular hump observed at 40 ° incidence. In the SRS-02 sample the surface domains have undergone a strong roundness, so only some particular incidence angles could provide efficient multiple reflections of light; in all other cases, there should be always a significant specular component. The micro-roughness introduced by carbon black grains, whose average size is around 700 Å, should not have any effect on light trapping.

6. Conclusions

Spectralon Labsphere standards with different nominal reflectance were characterized by investigating their optical, morphological and structural properties. The optical characterizations were performed analyzing the angle-resolved total reflectance at different wavelengths, the intensity and polarization of the diffused light as function of the scattering angle. The results of optical measurement show that higher is the nominal reflectance of the standard, better is its behavior as Lambertian diffuser. The reason for this is that the average reflectance of a standard is obtained by mixing a fluoropolymer, of very high reflectivity and highly diffusing, with various amounts of carbon black particles, highly absorbing and with smooth surface. As a consequence, the SRS-02 standard, of 2% nominal reflectance, is the farthest from the Lambertian behavior, whereas the SRS-99 standard, of 99% nominal reflectance, and made of pure fluoropolymer, shows the best optical properties and can be considered, in practice, an ideal Lambertian diffuser. The standards with reflectance between 2% and 99% show optical properties intermediate between these two extremes. Despite this, it is possible to find, for any standard, the restricted conditions in which each of them can work as a Lambertian diffuser. All the standards therefore can find applications in optical apparatus, provided that their use be made taking account of their properties, as found by this study, and the limitations imposed by the experimental conditions.

REFERENCES

[1] G. Kortum, J.E. Lohr, Reflectance Spectroscopy. Principles, Methods, Applications (Berlin, Heidelberg, New York, Springer, 1969).

[2] ASTM E 1175-87, Standard Test Method for Determining Solar or Photopic Reflectance, Transmittance and Absorptance of Materials Using a Large Diameter Integrating Sphere, American Society for Testing and Materials, PA, USA, 1987 (also reapproved, 1996).

[3] A. Maccari, M. Montecchi, F. Treppo, M. Zinzi, CATRAM, An apparatus for the optical characterization of advanced transparent materials, Appl. Opt. 37 (1998) 51-56.

[4] A. Parretta, A. Sarno and H. Yakubu, "Non-destructive Optical Characterization of Photovoltaic Modules by an Integrating Sphere. Part I: Mono-Si Modules", Optics Communications, 161 (1999) 297-309.

[5] A. Parretta, A. Sarno, P. Tortora, H. Yakubu, P. Maddalena, J. Zhao, A. Wang, "Angle-dependent Reflectance and Transmittance Measurements on Photovoltaic Materials and Solar Cells", Optics Communications, 172 (1999) 139-151.

[6] A. Parretta, P. Grillo, P. Tortora and P. Maddalena, "Method for Measurement of the Directional/Hemispherical Reflectance of Photovoltaic Devices", Optics Communications, 186 (2000) 1-14.

[7] A. Parretta, H. Yakubu, F. Ferrazza, "Method for Measurement of the Hemispherical/Hemispherical Reflectance of Photovoltaic Devices", Optics Communications, 194 (2001) 17-32.

[8] P. Maddalena, A. Parretta, A. Sarno and P. Tortora, "Novel Techniques for the Optical Characterization of Photovoltaic Materials and Devices", Optics and Lasers in Engineering, 39 (2003) 165-177.

[9] A. Parretta, P.P. Altermatt and J. Zhao, "Transmittance from Photovoltaic Materials under Diffuse Light", Solar Energy Materials and Solar Cells, 75 (2003) 387-395.

[10] P. Maddalena, A. Parretta, P. Tortora, P. Altermatt and J. Zhao, "Simultaneous Optical Losses and Current Measurements in Photovoltaic Devices at Variable Angle of the Incident Light", Solar Energy Materials and Solar Cells, 75 (2003) 397-404.

[11] A. Parretta, H. Yakubu, F. Ferrazza, P.P. Altermatt, M.A. Green and J. Zhao, "Optical Loss of Photovoltaic Modules under Diffuse Light", Solar Energy Materials and Solar Cells,

75 (2003) 497-505.

[12] A. Parretta, P. Grillo and M. Tucci, “Investigation of minority carrier diffusion length in shallow junctions by angle-resolved illumination technique”, Materials Science and Engineering B, 102 (2003) 179-183.

[13] A. Parretta, G. Graditi, R. Schioppo, M. Bombace, “Optical degradation of long-term field-aged c-Si photovoltaic modules”, Solar Energy Materials and Solar Cells, 86 (2005) 349-364.

[14] A. Parretta, “Riflettometro per la mappatura ottica di una superficie di un articolo”. Patent It. N. 0000263666, 01 dicembre 2009.

[15] P. Morvillo, E. Bobeico, A. Parretta, “Scatterometro a sfera integratrice, sensore di posizione e dimensione di oggetti, e relativi metodi di misura”. Patent It. N. 0001359566, 24 aprile 2009.

[16] S. Granata e A. Parretta, “Apparecchio per la riproduzione della figura di diffusione della luce da campioni fotovoltaici”. Patent It. N. 0001323778, 28 settembre 2004.

[17] P. Maddalena, A. Parretta, P. Tortora, “Apparecchio e metodo per la misura simultanea della corrente e della riflettanza di una cella solare”. Patent It. N. 0001323346, 16 agosto 2004.

[18] F. Ferrazza, A. Parretta, S. Pietruccioli, A. Sarno, M. Tucci, “Apparecchio e metodo per la caratterizzazione ottica in luce diffusa di materiali e dispositivi fotovolataici”. Patent It. N. 0001316247, 03 aprile 2003.

[19] A. Parretta, A. Sarno, P. Tortora, “Apparecchio e metodo per la misura differenziale della riflettanza di una superficie”. Patent It. N. 0001307587, 14 novembre 2001.

[20] A. Parretta, "Dispositivo per la esecuzione non distruttiva di misure di riflettanza spettrale, globale, speculare e diffusa, ad angolo di incidenza variabile, nonch è di trasmittanza, per celle solari e moduli fotovoltaici". Patent It. N. 0001295845, 28 maggio 1999.

[21] E. Bobeico, F. Varsano, F. Roca and A. Parretta, “Light Backscattering Properties of Textured Silicon Materials”, Proc. of the National Conference on Physics of Matter, INFM Meeting 2001, Rome, Italy, 18-22 June, 2001. INFM, Rome, 2001, p. 242.

[22] A. Parretta, “Camera for recording light backscattered from textured photovoltaic samples”, 19th Congress of Int. Commission for Optics, ICO XIX, Optics for the Quality of Life”, Firenze, 25-30 August 2002. Technical Digest ed. by A. Consortini and G.C. Righini 2002, pp. 831-832. Proc. of SPIE - The Int. Soc. for Optical Engineering, Washington, USA: SPIE Vol 4829 II, 2003, pp. 856-858.

[23] E. Bobeico, L. Lancellotti, P. Morvillo, A. Parrettta, A. Wang and J. Zhao, “Analysis of Light Backscattering from Textured Silicon Surfaces”, Conference “PV in Europe, from PV Technology to Energy Solutions”, Rome, Italy, 7-11 October 2002. Ed. J.L. Bal, G. Silvestrini, A. Grassi, W. Palz, R. Bigotti, M. Gamberane, P. Helm. WIP-Munich and ETA-Florence, 2002, pp. 268-271.

[24] A. Parretta, E. Bobeico, L. Lancellotti, P. Morvillo, A. Wang and J. Zhao, “A new approach to the analysis of light collection by textured silicon surfaces”, Proc. of the 3rd World Conference on Photovoltaic Energy Conversion, Osaka, Japan, 7-11 May, 2003. Vol. A, 2003, pp. 122-125.

[25] A. Parretta, “Camera for recording light backscattered from photovoltaic devices”, Journal of Optics B, Pure and Applied Optics, 5 (2003) S1-S9.

[26] A. Luque, G. Sala, J. C. Arboiro, T. Bruton, D. Cunningham, and N. Mason, “Some results of the EUCLIDES photovoltaic concentrator prototype,” Prog. Photovolt. Res. Appl. 5 (1997) 195–212.

[27] I. Antón, D. Pachón, and G. Sala, “Characterization of optical collectors for concentration photovoltaic applications,” Prog. Photovolt. Res. Appl. 11 (2003) 387–405.

[28] A. Parretta, C. Privato, G. Nenna, A. Antonini, M. Stefancich, “Monitoring of concentrated radiation beam for photovoltaic and thermal solar energy conversion applications”, Applied Optics, 45 (2006) 7885-7897.

[29] Labsphere, Inc., 231 Shaker St., North Sutton, NH03260, USA, www.labsphere.com.

[30] E.F. Zalewski: in Handbook of Optics, ed. M. Bass (McGraw-Hill, New York, 2001) Vol. II, p. 24.3.

[31] J. Jacquez, H.F. Kuppenheim, Theory of the Integrating Sphere, J. Opt. Soc. Am. 45 (1955) 460-470.

[32] Labsphere Inc., 1994, A Guide to Integrating Sphere Theory and Applications, www.labsphere.com.

[33] Labsphere Inc., 1994, A Guide to Integrating Sphere Radiometry and Photometry, www.labsphere.com.

[34] Hoffman Sphere Optics, 2007, Integrating Sphere Design and Applications Technical Information, www.sphereoptics.com.